**FINAL TECHNICAL REPORT**

| | |
|---|---|
| DOE Award: | DE-FC26-06NT43024 |
| Name of recipient: | Louisiana State University, Baton Rouge, LA |
| Project Title: | "Catalytic Process for the Conversion of Coal-derived Syngas to Ethanol" |
| Principle Investigator: | James J. Spivey, Louisiana State University |
| Co-Principle Investigators: | Doug Harrison and John Earle, Louisiana State University<br>James G. Goodwin, Jr., David Bruce, Xunhua Mo, Walter Torres, (Clemson)<br>Joe Allison,Vis Viswanathan, Rick Sadok (Conoco-Phillips),<br>Steve Overbury and Viviana Schwartz (ORNL) |
| Date of Report: | August 16, 2011 |
| Period covered by report: | Sept 30, 2006 – July 29, 2011 |

**Disclaimer**

**Table of Contents**

# Executive Summary

**Rationale.** The catalytic conversion of coal-derived syngas to $C_{2+}$ alcohols and oxygenates has attracted great attention due to their potential as chemical intermediates and fuel components. This is particularly true of ethanol, which can serve as a transportation fuel blending agent, as well as a hydrogen carrier.

**Thermodynamics**. A thermodynamic analysis of CO hydrogenation to ethanol that does not allow for byproducts such as methane or methanol shows that the reaction:

$$2\ CO + 4\ H_2 \rightarrow C_2H_5OH + H_2O$$

is thermodynamically favorable at conditions of practical interest (e.g,30 bar, <~250°C). However, when methane is included in the equilibrium analysis, no ethanol is formed at any conditions even approximating those that would be industrially practical. This means that undesired products (primarily methane and/or $CO_2$) must be kinetically limited. This is the job of a catalyst.

**Catalysts**. The mechanism of CO hydrogenation leading to ethanol is complex. The key step is the formation of the intial C-C bond. Catalysts that are selective for EtOH can be divided into four classes: (a) Rh-based catalysts, (b) promoted Cu catalysts, (c) modified Fischer-Tropsch catalysts, or (d) Mo-sulfides and phosphides. This project focuses on Rh- and Cu-based catalysts. The logic was that (a) Rh-based catalysts are clearly the most selective for EtOH (but these catalysts can be costly), and (b) Cu-based catalysts appear to be the most selective of the non-Rh catalysts (and are less costly). In addition, Pd-based catalysts were studied since Pd is known for catalyzing CO hydrogenation to produce methanol, similar to copper.

**Approach.** The overall approach of this project was based on (a) computational catalysis to identify optimum surfaces for the selective conversion of syngas to ethanol; (b) synthesis of surfaces approaching these ideal atomic structures, (c) specialized characterization to determine the extent to which the actual catalyst has these structures, and (d) testing at realistic conditions (e.g., elevated pressures) and differential conversions (to measure true kinetics, to avoid deactivation, and to avoid condensable concentrations of products in the outlet gas).

**Key Results—Rh catalysts**. The effects of synthesis methods, promoters, and reaction variables were studied. The doubly promoted 1.5% Rh–La/V/$SiO_2$ catalyst exhibited the highest activity and selectivity towards ethanol formation. An ethanol selectivity of 52%, with a corresponding methane selectivity of 15.4% and a CO conversion of 7.5%, was achieved on this Rh-La/V/$SiO_2$ catalyst at 14 bar, 270 °C and $H_2$/CO=2. This selectivity is nearly equal to the highest value reported in the literature -- which is 56% for a catalyst containing 6% Rh and tested at 54 bar. The high selectivity of this catalyst appears to be due to a synergistic promoting effect of lanthana and vanadia, modifying both chemisorption and catalytic properties. Interestingly, on our catalyst (contrary to literature studies), pressures higher than 14 bar led to a dramatic increase in methane selectivity at the expense of ethanol. This pressure of 14 bar would couple more easily with a coal gasifier than the higher pressure required to reach the only slightly higher selectivity.

**Key Results—Cu catalysts**. Modified copper based catalysts including novel core-shell type bimetallic nanoparticles, rare earth oxide pyrochlores and electrodeposited nanowires were synthesized and tested. Uniformly dispersed and highly reproducible core-shell nanoparticles were synthesized which exhibited optical, magnetic and catalytic properties. Design of such core-shell nanostructures is anticipated to pave way for the development of novel materials with combined optical, magnetic and catalytic properties. The highest EtOH selectivity on Cu-based catalysts was 18% with negligible methane on Cu-Mn-ZnO-$La_2Zr_2O_7$-$Li_2O$ pyrochlores at 230 °C, 20 bar, $H_2$/CO=2 and 18,000 scc/(h gcat). The total alcohol selectivity (including MeOH and all higher alcohols) was 57% on this catalyst which is greater/comparable to those on the few Cu-based catalysts reported in literature. A direct comparison to Cu-based catalysts reported in the literature requires reporting our total alcohol selectivity on a $CO_2$-free basis (which results in a larger value for selectivity than the same calculation reported as "carbon selectivity"—which we use to report all values in our published papers and in the project Final Report). Using the $CO_2$-free basis, the total alcohol selectivity for our Cu-based catalysts was >90%, which is greater than any value reported in literature.

**Key Results—Computational catalysis**. DFT calculations were performed to study the adsorption of CO and $H_2$ on small rhodium clusters. The results indicate that the initial adsorbate position parallel to one of the cluster three-fold faces is highly favorable for $H_2$ chemisorption consistent with previous calculations on metallic periodic surfaces, and the energy of CO adsorption on the three-fold sites decreases with the number of metal atoms in the cluster and adsorption on the terminal and bridge sites becomes dominant. When CO is adsorbed on rhodium cluster ($Rh_7$) pre-adsorbed with $(H)_2$, an increase in the average H-Rh bond length ensues suggesting that H atoms become more available for further reaction.

DFT studies also showed that the adsorption of methanol, ethanol and acetaldehyde on small rhodium clusters through the oxygen atom was in qualitative agreement with a Lewis acid-base interaction in which the alcohols and the aldehyde act as the base and the metal surface as the acid.

**Key Results—Economics**. Two preliminary process economic analyses of a commercial scale plant based on 10,000 tons/day coal feed were carried out using: (a) the Cu-Mn-ZnO-$La_2Zr_2O_7$-$Li_2O$ and (b) the 1.5%Rh–La/V/$SiO_2$ catalyst. A conceptual 10,000 TPD Coal-to-Ethanol plant was simulated to evaluate the economic impact of varying the performance of several process variables associated with the ethanol reactor.

For the Rh-based catalyst, the production cost of ethanol (without subsidy) ranged from $2.20 to $3.70/gal (depending on assumptions), which is competitive with current market costs and to costs estimated by DoE for thermochemical processes (Phillips et al., NREL/TP-510-41168, April 2007). However rhodium is more costly than platinum or gold (~$1,100 per troy ounce Rh), due to which a reactor design that minimizes the required catalyst inventory is critical to the economics of this project. Another important factor was complete regeneration of the catalyst. As a result, non-Rh based catalysts were explored and process economic analysis was carried out on a Cu-Mn-ZnO-$La_2Zr_2O_7$-$Li_2O$ pyrochlore-based catalyst.

For the Cu-pyrochlore catalyst, the unexpectedly high cost of lanthanum dominates the cost of the catalyst, making up 89% of the catalyst cost. With the cost of lanthanum estimated to be $210/kg, coupled with the fact that methanol (rather than the more valuable $C_{2+}$ alcohols), comprises 80 liquid volume % of all alcohols produced, a plant build upon this technology would fall well short of economic viability. For a conceptual plant that feeds syngas produced by the gasification of 10,000 TPD of Illinois #6 coal to achieve breakeven economics, the ethanol, which makes up only 17 LV% of the alcohols produced, would have to sell for $11.13/gallon. This compares to ethanol's current market price of ~$2.50/gallon.

**Financial Report:** The Cost Plan/Status report is shown in Appendix I.

**Milestone status**: The planned and actual Milestones are below:

| Task | Critical Path Project Milestone Description | Planned Start Date | Actual Start Date | Planned End Date | Actual End Date |
|---|---|---|---|---|---|
| 2.0 | Initial computational simulations | 10/06 | 10/06 | 6/07 | 6/07 |
| 3.0 | Catalyst synthesis | | | | |
| | 3.1 Baseline | 10/06 | 10/06 | 12/06 | 12/06 |
| | 3.2 Rh-based catalysts | 12/06 | 12/06 | 03/08 | 03/08 |
| | 3.3 Cu-based catalysts | 03/07 | 03/07 | 03/08 | 03/08 |
| 9.0 | Activity testing | 03/07 | 03/07 | 03/11 | 03/11 |
| 10.0 | Interim simulation/economics | 03/08 | 03/08 | 12/08 | 12/08 |
| 13.0 | Extended tests of catalysts | 09/10 | 09/10 | 06/11 | 06/11 |
| *14.0* | Final process simulation/economics | 12/10 | 12/10 | 06/11 | 06/11 |

## Results and Discussion: Rhodium-based catalysts

### (1) Lanthana and vanadia promoted $Rh/SiO_2$ catalysts

The effect of various promoters on supported Rh catalysts was investigated. A series of La and/or V oxide promoted $Rh/SiO_2$ catalysts, namely unpromoted $Rh(1.5)/SiO_2$, singly promoted catalysts $Rh(1.5)–La(2.6)/SiO_2$ and $Rh(1.5)/V(1.5)/SiO_2$, and a doubly promoted catalyst $Rh(1.5)–La(2.6)/V(1.5)/SiO_2$, was prepared using the incipient wetness impregnation method. Powder X-ray diffraction and TEM results suggested that Rh, lanthana and vanadia were all highly dispersed in the promoted $Rh/SiO_2$ catalysts, with no Rh particles distinguishable in TEM images. CO chemisorption and FT-IR studies indicated significantly different CO adsorption behaviors of the different catalysts. V promotion decreased CO adsorption while La promotion showed the opposite effect. Compared to the singly promoted catalysts $Rh–La/SiO_2$ and $Rh/V/SiO_2$, the doubly promoted $Rh–La/V/SiO_2$ catalysts exhibited higher activity and better selectivity towards ethanol formation. The catalytic performance of the $Rh–La/V/SiO_2$ catalyst was not affected significantly by increasing the V content beyond V/Rh = 2; however, La promotion greater than La/Rh = 2 resulted in less desirable catalytic properties. The high ethanol yield of the $Rh–La/V/SiO_2$ catalysts appears to be due to a synergistic promoting effect of lanthana and vanadia, modifying both chemisorption and catalytic properties.

The doubly promoted $Rh–La/V/SiO_2$ catalyst showed 20% EtOH selectivity (balance primarily hydrocarbons) at 1.8 atm (Table 1), which is much greater than any combination of the promoters individually (or unpromoted Rh). Recent literature results on Mn promoted Rh/silica showed 61% selectivity to EtOH (34% to $CH_4$, 2% to MeOH) at 53 atm [1].

Table 1: Catalytic activities of Rh based catalysts[1]

| Catalyst | SS[b] rate (μmol/(g s)) | SS selectivity (%)[c] | | | | | | $C_2^=/C_2$ | $C_3^=/C_3$[d] |
|---|---|---|---|---|---|---|---|---|---|
| | | $CH_4$ | $C_{2+}HC$[e] | MeOH | Acetaldehyde | EtOH | Other $C_{2+}$ oxy.[f] | | |
| $Rh(1.5)/SiO_2$ | 0.03 | 48.1 | 28.7 | 1.2 | 6.5 | 15.6 | – | 1.8 | 12.0 |
| $Rh(1.5)–La(2.6)/SiO_2$ | 0.09 | 35.3 | 32.0 | 3.2 | 5.8 | 23.6 | – | 1.2 | 3.3 |
| $Rh(1.5)/V(1.5)/SiO_2$ | 0.09 | 12.5 | 66.8 | 5.0 | 2.1 | 12.5 | 1.3 | 4.8 | 10.3 |
| $Rh(1.5)–La(2.6)/V(1.5)/SiO_2$ | 0.29 | 16.2 | 50.8 | 1.8 | 5.4 | 20.8 | 4.9 | 3.3 | 12.1 |

[a] Catalyst: 0.3 g; inert: α-alumina 3 g; pretreatment: 500 °C in $H_2$; reaction conditions: $T = 230$ °C, $P = 1.8$ atm, flow rate = 45 mL/min ($H_2/CO = 2$). Data taken at 15 h TOS after steady state reached. Error = ±5% of all the values measured except for $Rh(1.5)/SiO_2$ which was ±10% due to low activity.

[b] Steady state.

[c] Carbon selectivity $= n_i C_i / \sum n_i C_i$.

[d] $C_n^=/C_n$ is the ratio of $C_n$ olefin selectivity to $C_n$ paraffin selectivity ($n = 2, 3$).

[e] Hydrocarbons with 2 or more carbons.

[f] Oxygenates with 2 or more carbons, not indicating acetaldehyde and ethanol.

[1] Gao et al., *J. Catal*. 262 (2009) 119

**(2) Role of promoters on CO hydrogenation of $Rh/SiO_2$ catalysts**

On the contrary to La and V, the addition of Zn and Cu dramatically reduced the reaction activity of $Rh/SiO_2$ for CO hydrogenation. The effects of La, V, Zn and Cu on $Rh/SiO_2$ catalyst for CO hydrogenation were investigated using DRIFTS at atmospheric pressure. While La enhanced total CO adsorption, the addition of V, Zn and Cu suppressed the CO adsorption to different extents. The infrared study of CO desorption and hydrogenation on different catalysts indicated that the linear Rh-CO [CO(l)] and the tilted Rh-CO [CO(t)] might be more active while the bridged $Rh_2CO$ [CO(b)] and $Rh_2(CO)_3$ [CO(bd)] might be less active for the reaction. The addition of V appeared to enhance the desorption rate and/or reactivity of CO on the catalytic surface, while the addition of La may have created new active sites for the reaction. For the doubly promoted catalyst $Rh\text{-}La/V/SiO_2$, it appeared to have more active sites to adsorb CO than the V singly promoted catalyst and the adsorbed CO species appeared to be more active than those on the La singly promoted catalyst. On the contrary, the addition of Zn or Cu significantly reduced the desorption rate and/or reactivity of CO on the catalytic surface, resulting in poor performances for CO hydrogenation [2].

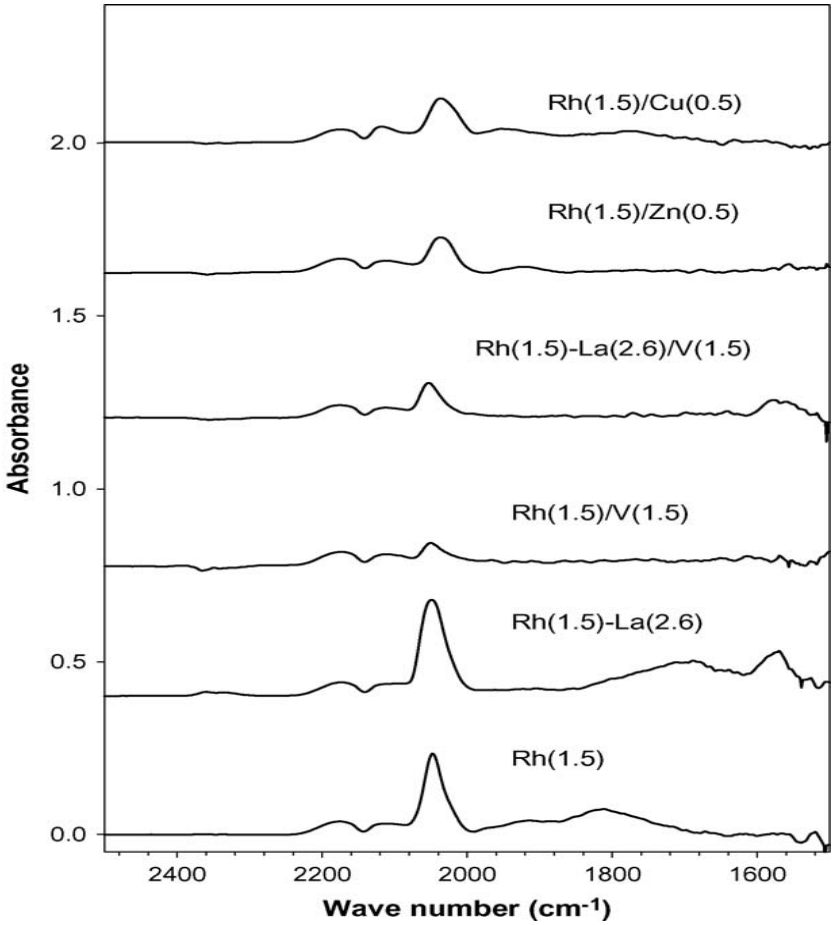


Figure 1: DRIFTS spectra after CO hydrogenation on different catalyst at 230 °C for 30 min[2]

[2] Mo et al., *Catal. Today* 147 (2009) 139

It was found that Rh and promoters were highly dispersed and apparently in close contact. The addition of promoters hindered the reduction of Rh and changed CO and $H_2$ adsorption behaviors on the catalyst surfaces. It was also found that the addition of 0.8 wt% Fe, 2.6 wt% La, and 1.5 wt% V to 1.5 wt% $Rh/SiO_2$ resulted in the highest selectivity to ethanol (34.6%) and a moderate activity compared to other promoted catalysts at the reaction conditions of 230°C and 1.8 atm. The various characterization results and the catalytic behaviors of different catalysts suggest that the main effect of La promotion was to increase CO adsorption and CO insertion, the main effect of the addition of V was to decrease CO adsorption but to enhance CO dissociation and hydrocarbon chain growth, while the main effect of the addition of Fe was to decrease CO adsorption and enhance hydrogenation. The synergistic effects of multiple promoters imply that the key to effective catalyst design for ethanol synthesis from syngas is a balance among CO dissociation, hydrogenation, and CO insertion[3]. The effect of Fe loading on the CO hydrogenation properties of $Rh\text{-}La\text{-}Fe/V/SiO_2$ catalyst is shown in Figure 2.

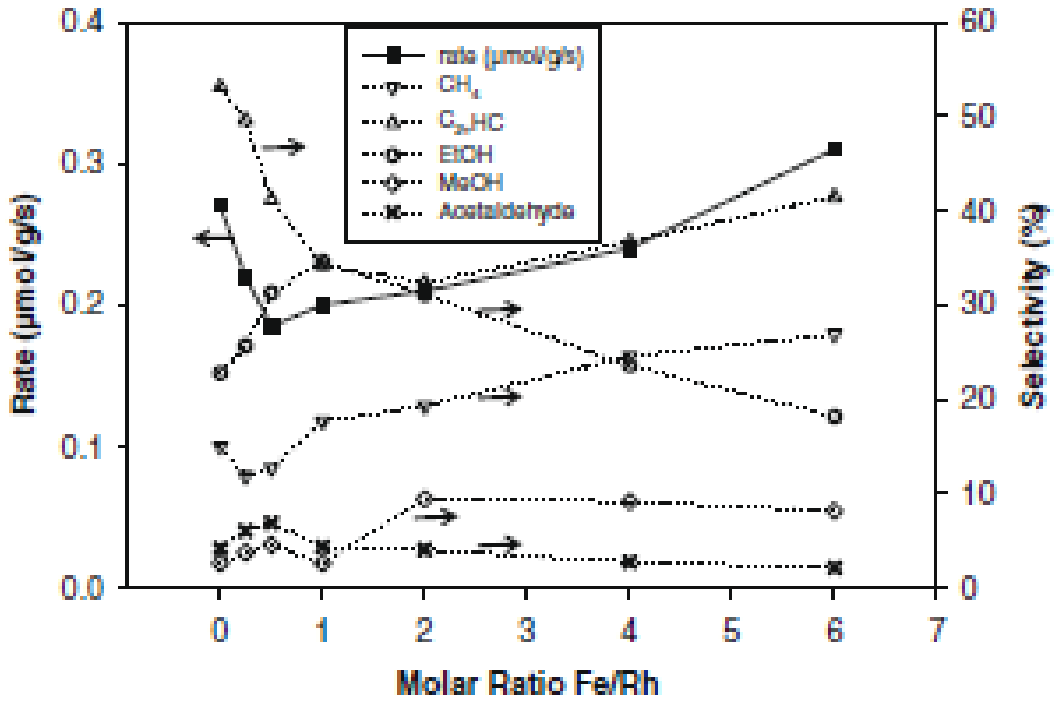


Figure 2: Effect of Fe loading on the catalytic properties of $Rh\text{-}La\text{-}Fe/V/SiO_2$ [3]

**(3) Kinetic study of $Rh/SiO_2$ catalysts**

A kinetics study of CO hydrogenation on these catalysts was conducted to understand the mechanism and the role of promoters. All the catalysts except RhFe and RhLaFeV showed the same trends in CO conversion and selectivities to different products with increasing CO or H2 partial pressure. The influence of partial pressure to activity is more obvious for RhLaV than for other catalysts, which appears due to a synergistic promoting effect of La and V. For the Fe-



[3] Mo et al., *J. Catal*. 267 (2009) 167

promoted catalysts, the CO conversion rate increases with CO partial pressure, which may be because Fe serves like a reservoir to hydrogen on the catalyst surface. The parameters obtained from power law were used to fit the rate expressions derived based on different limiting steps to understand the reaction mechanism and the effects of different promoters. The fact that coefficient x is positive and the coefficient y is negative indicates promotion by hydrogen and inhibition by carbon monoxide. By comparing the power-law parameters with the Langmuir–Hinshelwood rate expression, CHO-S + H-S<->$CH_2O$ + S (where S refers to surface) is more likely to be the rate-limiting step for the methane formation on Rh and RhLa. The rate-limiting step for the methane formation on RhV and RhLaV is $CH_2O$-S + H-S<->$CH_3O$-S + S or $CH_3O$-S + S<->$CH_3$-S +O-S. For ethanol synthesis, $C_2H_5O$-S + H-S<->$C_2H_5OH$ + 2S is the possible rate-limiting step for all the catalysts except for RhFe. However, it is unclear that whether $CH_3$-S + $CH_2O$-S<->$C_2H_5O$-S + S or $C_2H_5O$-S + H-S<->$C_2H_5OH$ + 2S is the rate-limiting step for ethanol synthesis on RhFe [4].

Table 2: Activation energy for the synthesis of $CH_4$, $C_2H_n$, $C_3H_n$, EtOH and total CO conversion[4]

| Catalysts | CO conversion | $CH_4$ formation | $C_2H_n$ formation | $C_3H_n$ formation | EtOH formation |
|---|---|---|---|---|---|
| Rh | 25.6 | 29.2 | 29.6 | 24.3 | 18.3 |
| RhLa | 27.4 | 31.6 | 30.2 | 30 | 24.2 |
| RhFe | 21.5 | 23.9 | 22.6 | 23 | 15.7 |
| RhV | 26.9 | 30.9 | 28.5 | 28.5 | 17.6 |
| RhLaV | 27.4 | 30.5 | 28.4 | 29.5 | 21.3 |
| RhLaFeV | 25.3 | 28.2 | 27.6 | 27.4 | 21.5 |

[a] Catalyst: 0.3 g; Inert: α-alumina 3 g; Pretreatment: 500 °C in $H_2$; Data taken at 15 h TOS after steady state was reached.

[b] At constant flow rate = 45 mL/min ($H_2$/CO = 2), $P$ = 1.8 atm, the activation energy for each catalyst is determined by $\ln r = \ln A - \frac{E_a}{RT}$ while temperature varied from 210 to 270 °C.

[c] Error = ±10% for all the values measured.

[d] The unit of activation energy is kcal/mol.

**(4) SSITKA analysis of promoted Rh/$SiO_2$ catalysts**

Strong metal-oxide interactions (SMOI) effects caused by V promotion significantly modified CO hydrogenation on Rh/$SiO_2$. Using SSITKA, surface kinetic parameters were able to be determined, which permits a better understanding of the surface modification of the catalyst by SMOI. It has been concluded based on the data for Rh/$SiO_2$ and TEM results for Rh/V/$SiO_2$ that sintering of Rh does not occur for reduction temperatures from 300 to 600°C. $H_2$ chemisorption indicated that $H_2$ adsorption at room temperature is suppressed with V addition. The product distribution for FTS on Rh/$SiO_2$ was constant with rising reduction temperature except for hydrocarbon chain growth which was somewhat improved. However, for Rh/V/$SiO_2$, the overall catalyst activity decreased significantly with increasing reduction temperature because of detrimental SMOI effects. Also, there was a shift between methane and methanol selectivities with increasing reduction temperature. As indicated by SSITKA, the site activity of V-promoted



[4] Gao et al., *J. Catal*. 268 (2009) 142

$Rh/SiO_2$ was enhanced with higher reduction temperature. However, as shown also by SSITKA, SMOI effects decreased the concentration of active intermediates, which caused a decrease in overall activity by more than compensating for the increase in site activity. The reaction and SSITKA results are consistent with the formation of a partial $VO_x$ overlayer on the Rh surface and of new sites with higher activity being created probably at the $Rh–VO_x$ interface due to the SMOI effects [5].

Table 3: Effect of reduction temperature on surface reaction kinetic parameters at steady-state methanation conditions[5]

| Catalyst | Reduction temperature (°C) | SS rate (μmol/gcat/s)[a] | $CH_4$ selectivity (%) | $\tau_{CO}$ (s) | $N_{CO}$ (μmol/gcat)[b] | $\tau_{CH_4}$ (s) | $TOF_{ITK}$ ($s^{-1}$)[b] | $N_{CH_4}$ (μmol/gcat)[c] |
|---|---|---|---|---|---|---|---|---|
| $Rh/SiO_2$ | 300 | 0.038 | 98.4 | 8.38 | 15.42 | 9.81 | 0.10 | 0.39 |
| | 600 | 0.040 | 99.8 | 8.75 | 16.10 | 9.52 | 0.11 | 0.38 |
| $Rh/V/SiO_2$ | 300 | 0.048 | 90.2 | 4.98 | 9.04 | 5.77 | 0.17 | 0.25 |
| | 400 | 0.039 | 93.6 | 3.90 | 7.11 | 4.50 | 0.22 | 0.17 |
| | 500 | 0.029 | 84.8 | 2.42 | 4.42 | 2.69 | 0.37 | 0.07 |
| | 600 | 0.022 | 79.1 | 0.62 | 1.13 | 0.63 | 1.59 | 0.01 |

[a] Steady-state rate where rate is in μmol CO converted/gcat/s. Catalyst: 0.3 g, inert: α-alumina 3 g; reaction at 280 °C; $P$ = 1.8 atm, flow rate = 60 mL/min ($H_2$:He:CO = 20:19:1). Reaction conversion was less than 5% in all cases. Experimental error: ±10%.

[b] TOF based on SSITKA, calculated as $TOF_{ITK} = 1/\tau_{CH_4}$.

[c] $N_i = rate_i \times \tau_i$.

**(5) Effect of reaction conditions at higher pressures on $Rh/SiO_2$ catalysts**

As an extension of the work carried out at Clemson University at 1.8 atm, the promoted $Rh/SiO_2$ catalysts were tested for CO hydrogenation at higher pressures in LSU. The focus was to investigate the impact of temperature, pressure, $H_2$/CO ratio and space velocity on the activity and selectivity of the lanthanum and/or vanadium oxide promoted $Rh/SiO_2$ catalysts. The formation of undesired methane could be suppressed under conditions of relatively high temperature, low pressure and low $H_2$/CO ratio. For the most active $Rh\text{-}La/V/SiO_2$ catalyst, these conditions were found to be 270 °C, 14 bar and $H_2/CO = 2$ and the highest ethanol selectivity achieved on this catalyst was 52%, with a corresponding methane selectivity of 15% at these conditions. Thus, combined La/V promotion seemed to alter the product distribution by increasing the rate of CO insertion, resulting in higher ethanol selectivities [6].

[5] Gao et al., *Catal. Today* 160 (2011) 44

[6] Subramanian et al., *J. Catal.* 272 (2010) 204

Table 4: Effect of H2/CO ratio on the product selectivities of Rh-La/V/SiO2 catalyst [6]

| Results | $H_2/CO = 2$ | $H_2/CO = 4$ |
|---|---|---|
| Rate of CO conversion (μmoles/gcat/s) | 2.9 | 3.2 |
| CO conversion (%) | 7.9 | 8.5 |
| *Selectivity (% C)* | | |
| $CO_2$ | 3.1 | 1.9 |
| $CH_4$ | 15.4 | 25.7 |
| MeOH | 5.0 | 6.9 |
| EtOH | 51.8 | 49.1 |
| $C_{2+}$ Oxy | 19.1 | 15.6 |
| $C_{2+}$ HC | 5.7 | 0.8 |

[a] Catalyst: 0.2 g; reaction conditions: $T = 270$ °C and $P = 14$ bar. 95% confidence limits (as absolute values) on selectivities are less than ±0.2% for all values except $CO_2$ (±1.5%) and $CH_4$ (±5%). Carbon balances are within 4% on all runs.

Ethanol and $C_{2+}$ oxygenate selectivity followed similar trends with space velocity, suggesting that they share a common intermediate, whereas methane and ethanol followed completely opposite trends indicating that they are formed by parallel reactions. Contrary to literature studies, higher pressures led to a dramatic increase in methane selectivity at the expense of ethanol, indicating increased CO dissociation activity at higher pressures, leaving fewer active CO molecules for insertion. The chain growth probability factors (α) for higher hydrocarbons and oxygenates were significantly different, suggesting that formation of these products could take place either due to different mechanisms or on different active sites. Less methanol was formed than would be expected by analysis of the chain growth distribution leading to $C_{2+}$ oxygenates, suggesting that methanol formation does not follow the same route as ethanol and other higher oxygenates. At the same time, more methane was formed than expected from the same analysis, suggesting that hydrogenation of surface $(CH_x)_{ads}$ species to methane takes place at a greater rate than $(CH_x)_{ads}$ participating in the ASF chain growth mechanism to form $C_{2+}$ hydrocarbons [6].

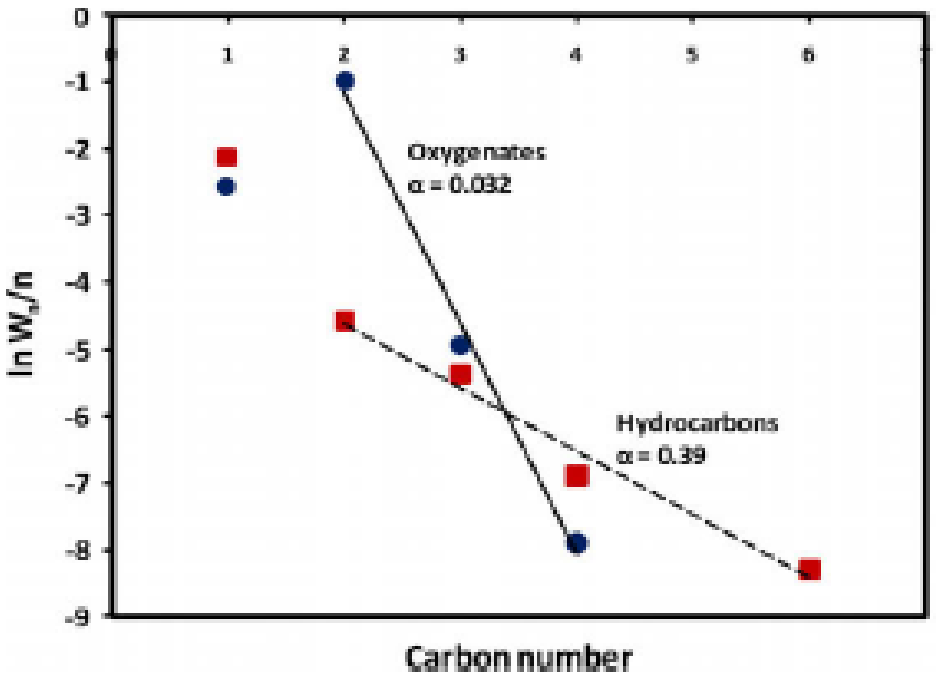


Figure 4: ASF plot for Rh-La/V/$SiO_2$ catalyst at 14 bar, 270 °C, $H_2$/CO=2 and S.V. = 9000 scc/(h gcat) [6]

**(2) Rh-Li catalysts for CO hydrogenation**

TPSR of CO and $H_2$ was conducted at 20 bar on a series of promoted Rh-$Al_2O_3$ catalysts The highest ethanol selectivity was given by RhLi-$Al_2O_3$ suggesting that it has the highest alcohol selectivity among the catalysts, while Rh-$Al_2O_3$ and RhMnLiFe-$Al_2O_3$ give the lowest intensity. Ethanol formation activity on both Rh-$Al_2O_3$ and RhMnLiFe-$Al_2O_3$ represents the two extreme cases amongst the catalyst tested – the CO dissociation activity is high on the Rh-$Al_2O_3$, leaving very few CO molecules for CO insertion. This in turn, leads to high methane activity. The RhMnLiFe-$Al_2O_3$ apparently inhibits the dissociation of CO, which minimizes methane formation, but also limits ethanol formation. RhLi-$Al_2O_3$ is an intermediate case (of CO dissociation activity), in which the presence of both dissociated and undissociated CO molecules results in the high ethanol activity [7].

[7] Egbebi et al., *Am. Chem. Soc.* 52 (2007)

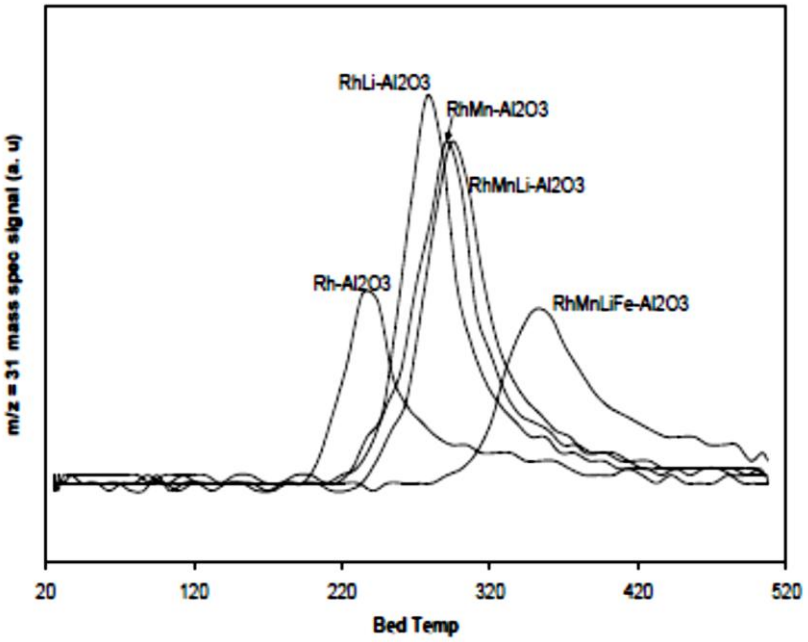


Figure 5: Ethanol formation profiles during TPSR of adsorbed CO and $H_2$ on promoted Rh-$Al_2O_3$ catalysts at 20 bar[7]

Steady state differential reaction studies on a series of 1 wt % Rh/$TiO_2$ catalysts promoted with Mn, Li, Fe shows significant differences in these promoters. Table 5 shows the selectivity of products for the CO hydrogenation reaction at 260 and 270 C on Rh/$TiO_2$ and Rh-Li/$TiO_2$ catalysts. The major products formed are methane, acetaldehyde, ethanol, methanol, some $C_2$-$C_3$ hydrocarbons along with traces of n-propanol and n-butanol. The selectivity and activity largely depend on Li promotion, although there are slight changes in selectivity patterns with temperature, even in the small temperature range explored. The CO conversion increases with temperature, as expected. Increasing the temperature increases the methane formation, while reducing the total oxygenates and ethanol selectivities.

Table 5: Products selectivity for CO hydrogenation over promoted Rh/$TiO_2$ catalysts (20 bar, 52800 scc/(h gcat), $H_2$/CO = 2) [8]

| | 260 °C | | 270 °C | |
|---|---|---|---|---|
| | Rh/$TiO_2$ | Rh–Li/$TiO_2$ | Rh/$TiO_2$ | Rh–Li/$TiO_2$ |
| Methanol | 6.8 | 3.7 | 5.5 | 2.8 |
| Acetaldehyde | 8.4 | 15 | 9.2 | 15 |
| Ethanol | 12 | 23 | 10 | 17 |
| Methane | 58 | 46 | 62 | 55 |
| $CO_2$ | 2.5 | 2.4 | 2.4 | 2.0 |
| $C_2^+$ hydrocarbons | 8.6 | 3.6 | 7.1 | 4.4 |
| Total oxygenates[a] | 30 | 47 | 28 | 38 |
| EtOH/total oxygenates | 0.40 | 0.49 | 0.37 | 0.43 |
| EtOH/$CH_4$ | 0.2 | 0.50 | 0.17 | 0.30 |
| Conversion, mol% C | 0.8 | 2.0 | 1.0 | 2.5 |

[a] Sum of oxygen containing products, excluding CO and $CO_2$.

[8] Egbebi et al., *Catal. Today* 149 (2010) 91

*In situ* IR/DRIFTS at ambient pressure and elevated temperatures was used to characterize the surface of $Rh/TiO_2$ catalysts and to investigate the effect of Li on the surface properties during CO and $CO_2$ hydrogenation. Under reaction conditions, there is no evidence of cationic Rh, since gem-dicarbonyl species are not observed in either Rh or Rh-Li supported catalyst. The presence of the Li promoter does not seem to alter the electronic structure of Rh, but rather it can introduce structural changes that could alter the Rh dispersion and/or bonding with CO. Several reaction products and intermediates could be observed on the surface. Water and CO clearly demonstrates the r-WGS path during $CO_2$ hydrogenation. Methane formation is particularly higher when $CO_2$ is present. Formation of oxygenated compounds could be observed and the features are more intense in the case of Li-promoted catalyst and CO hydrogenation. The Li promoter introduces a weakened CO adsorption site that appears to enhance the selectivity to $C_{2+}$ oxygenates. The selectivity to $C_{2+}$ oxygenates varies inversely with the reducibility of Rh metal, i.e., the lower the reducibility, the higher the selectivity.

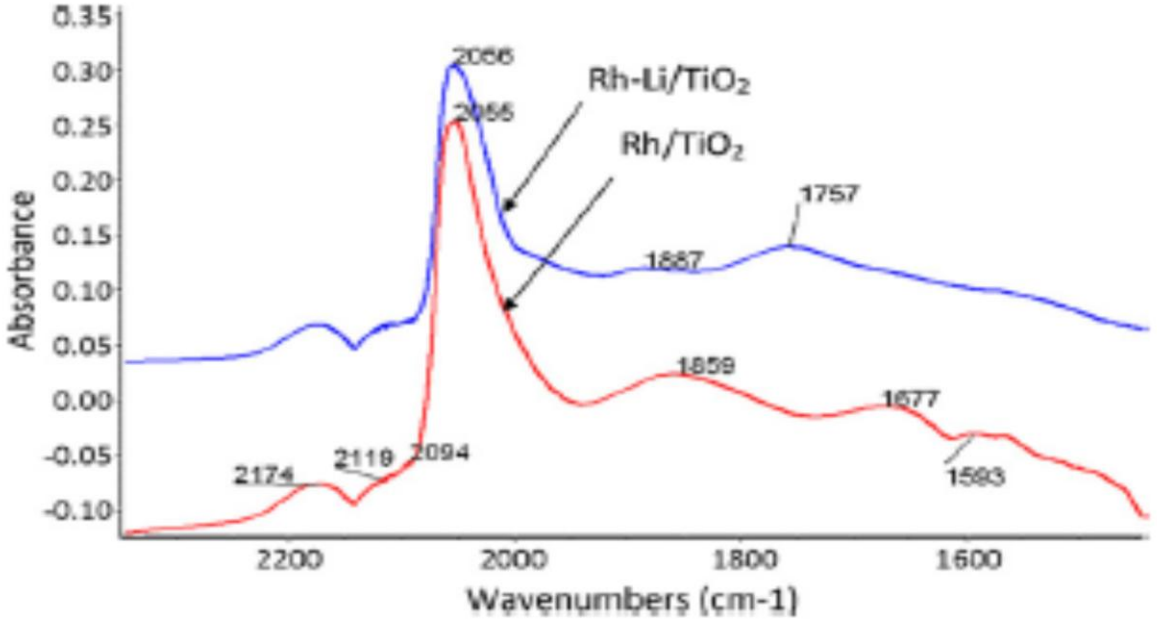


**Fig. 7.** Comparison of the FTIR spectra for CO adsorption at 270 °C over the pre-reduced $Rh/TiO_2$ and $Rh–Li/TiO_2$.

Figure 6: Comparison of FTIR spectra for CO adsorption at 270 °C over the pre-reduced $Rh/TiO_2$ and $Rh-Li/TiO_2$ catalysts [8]

# Results and Discussion: Copper based catalysts

## (1) Copper based core-shell nanoparticles

In the beginning stages of this research work, Co core-Cu shell and Co-Cu mixed (synthesized by simultaneous reduction of precursors) nanoparticles were studied as catalysts for CO hydrogenation. The highest ethanol selectivity achieved was 11.4% (with 17.2% methane selectivity) at differential conversions for the Co-Cu mixed nanoparticles [9]. The low selectivities towards ethanol and high selectivities towards hydrocarbons in the case of Co core-Cu shell nanoparticle catalyst may be either due to large concentrations of cobalt, an active Fischer Tropsch catalyst, resulting in an increased conversion of CO into hydrocarbons, or due to the excess surfactants on the catalyst surface which decompose at elevated reaction temperatures leaving carbon residues on the surface which affects the activity/selectivity of the catalyst.

The surfactant ligands may also block the adsorption sites, decreasing the active surface area available for catalysis and hence lead to a loss of catalytic activity. Thus, further modifications in the design of our core-shell nanoparticle catalysts were necessary in order to balance between the catalyst activity and selectivity to obtain a high yield of ethanol. Thus the later part of the project focused on reverse core-shell design: that is, copper being the primary core metal and the shell containing Mn or Co, with some changes in the synthesis method, and the surfactants retained on the nanoparticle surfaces after synthesis were removed before conducting the catalytic reactions.

### *Cu@$Mn_3O_4$ and Cu@$Co_3O_4$ core-shell nanoparticles:*

An organometallic wet-chemical synthesis approach was used to synthesize Cu core-Mn oxide shell (denoted as Cu@$Mn_3O_4$) and Cu core-Co oxide shell (denoted as Cu@$Co_3O_4$) nanoparticles using oleic acid and trioctylphosphine surfactants [10].

Figure 7 shows the HRTEM images of the as-prepared Cu@$Mn_3O_4$ and Cu@$Co_3O_4$ nanoparticles. The nanoparticles appear in spherical forms with distinguishable contrast between inner and outer regions suggesting core-shell structures. The particles are uniformly dispersed and show a narrow size distribution with a size of 13 ± 0.35 nm (for Cu@$Mn_3O_4$) and 11.4 ± 0.73 nm (for Cu@$Co_3O_4$). The Cu core size is ~6.1 nm and the shell is ~3.45 nm thick in the case of Cu@$Mn_3O_4$ nanoparticles, while the Cu@$Co_3O_4$ nanoparticles have a core of ~5 nm and a shell ~3.2 nm thick.

[9] Subramanian et al., *Catal. Today* 147 (2009) 100
[10] Subramanian et al., *J. Phys. Chem. C* 115 (2011) 14500

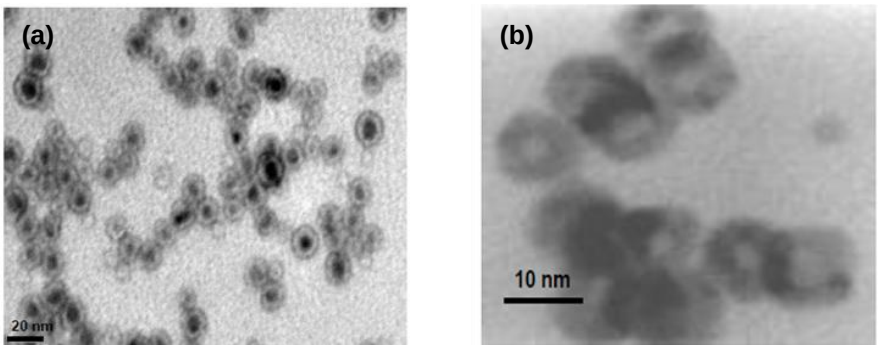

Figure 7: HRTEM images of the as-prepared nanoparticles (a) $Cu@Mn_3O_4$ and (b) $Cu@Co_3O_4$

DRIFTS showed that CO adsorbed in both linear and dicarbonyl forms on the ligand-free nanoparticles, and the desorbed CO as a result of He flushing over time led to the formation of surface bound carboxylate species, probably by reacting with the residual hydroxyl groups present after hydrogen reduction. The CO uptake was very high and the linearly adsorbed CO band was highly stable to He flushing on the $Cu@Mn_3O_4$ nanoparticles, indicating the presence of only $Cu^+$ active sites, whereas the partially stable linear carbonyl species on the $Cu@Co_3O_4$ nanoparticles indicated the possible presence of both $Cu^0$ and $Cu^+$ sites. The shift towards higher frequencies (blue-shift) in the case of $Cu@Mn_3O_4$ nanoparticles can be attributed to the lowering of the Lewis basicity (or electron density) of the surface Cu metal atoms by the presence of $Mn^{2+}$, consequently increasing the strength of the C≡O bond, which may result in an enhanced associative adsorption of CO during CO hydrogenation.

The effect of pressure on CO adsorption and hydrogenation was also studied using DRIFTS. Increase in the total pressure resulted in an increase in the intensity of the linear CO and an upward shift of its wavenumber. The linear CO uptake at 10 bar was roughly about 8 times greater than that at 1 bar. Hydrogenation of the pre-adsorbed CO at 270 °C indicated the disappearance of strongly pre-adsorbed linear CO in both $Cu@Mn_3O_4$ and $Cu@Co_3O_4$ nanoparticles, indicating the reaction of linear CO with $H_2$.

CO hydrogenation studies at 10 bar and 270 °C showed a highest ethanol selectivity of 15% on the $Cu@Co_3O_4$ nanoparticles with relatively low methane selectivity (10%), and a total alcohols/oxygenates selectivity of 47%. These results are in agreement with the DRIFTS results which indicated a lower CO dissociation activity on the $Cu@Mn_3O_4$ nanoparticles, and both dissociative and associative forms of CO adsorption on the $Cu@Co_3O_4$ nanoparticles, which may be the likely reason for higher selectivities towards alcohols/oxygenates on this catalyst.

**(2) Cu-ZnO and Mn Promoted Cu-ZnO nanowires prepared by electrodeposition**

CO stretching frequency was used to determine the extent of surface reduction of Cu-Zn and Mn-doped CuZn nanowires. The initial calcinations, performed to remove residual organics from the nanowires left an oxidized surface. FTIR showed that reduction at temperatures at least 320 °C is necessary to reduce surface Cu, for both the CuZn and the promoted Cu-Zn nanowires. CO adsorption studies do not reveal any clear differences in the reducibility between the promoted and unpromoted samples. Reduction steps at temperatures intermediate between 200 and 320 C will be necessary to differentiate an effect of Mn on the reduction temperature. The CO frequency after reduction at 320 C (2003 to 2014 cm-1) is too low to be due to adsorption on Cu metal. This was seen in studies of previously studied nanowires. The low frequency is attributed to Cu-Zn interaction. The position of the reduced species is slightly red-shifted slightly by the presence of Mn (from 2014 to 2003 cm-1), suggesting a weakening of the CO bond and possibly indicating a strengthening of the CO adsorption energy. Both of these may be favorable increased selectivity to oxygenate formation. TEM showed clearly that these samples exhibit nanowire morphologies. Previous nanowires studied by TEM did not exhibit such clear nanowire structures (see Progress report 2009 Q4). The nanowire walls are also quite porous and are composed of well-defined and highly aligned polycrystals. The phases present are presumably both ZnO and Cu. TEM showed that nanowires are ca. 400 nm think and 4-8 μm in lengths. Cu-Zn nanowires grow in one direction whereas Mn promoted growth has no specific direction. SAED showed that nanowires are polycrystalline.

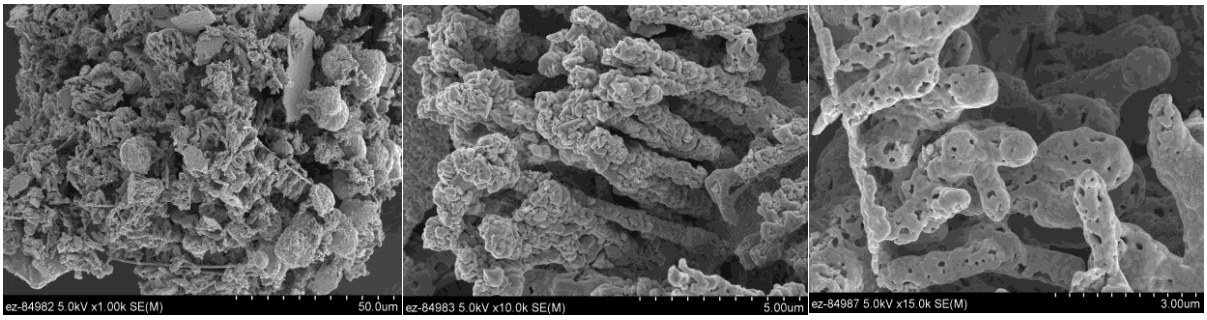

Figure 8: SEM images of Cu-Mn-ZnO nanowires

**(3) Transition metal promoted copper-rare earth zirconate catalysts**

A promising class of materials is based on rare earth zirconate supports with cubic pyrochlore structures, such as $La_2Zr_2O_7$, which have an excellent thermal and chemical stability towards deactivation and low sintering rates. This pyrochlore is believed to be a promising candidate as a support for a stable and active copper catalyst for $C_{2+}$ oxygenates synthesis. A series of transition metal promoted Cu-ZnO-$La_2Zr_2O_7$-$Li_2O$ catalysts were synthesized using coprecipitation. The structural and chemical changes in the local environment of Cu and the significance of transition metal promotion were investigated using *in-situ* X-ray diffraction (XRD) as well as synchrotron-

based X-ray absorption near-edge structure spectroscopy (XANES) experiments carried out under $H_2$-TPR conditions.

*In-situ* XRD and XANES studies under $H_2$-TPR conditions revealed that transition metal promoters (Mn and Co) increased the reducibility of copper in Cu-ZnO-$La_2Zr_2O_7$-$Li_2O$ (CZLL) catalysts. Once formed, metallic copper accelerated the reducibility of the Mn and Co oxides. TPR results indicated that the Mn or Co promoter also increased the overall extent of reduction of the catalysts, suggesting a synergistic interaction between Cu and Mn or Co. Room temperature XRD indicated the presence of crystalline phases of CuO, ZnO and $Co_3O_4$ on the framework of the pyrochlore lattice (phase rejection process), rather than being completely substituted into the pyrochlore structure. But manganese could be present only on the surface of the pyrochlore support, but was not detectible in XRD due to smaller particle size. *In-situ* XRD during $H_2$-TPR confirmed the formation of a cubic pyrochlore structure irrespective of the promoter metal used and the pyrochlore phase was found to be stable under high temperature activation conditions. Additionally, *in-situ* XANES experiments on the Cu K-edge of the catalysts allowed for a comparison of the reduction behavior of copper with the TPR and *in-situ* XRD results. This study emphasizes that the presence of copper sites in close proximity to the Mn or Co promoter atoms affects the dispersion and the reducibility of the catalyst.

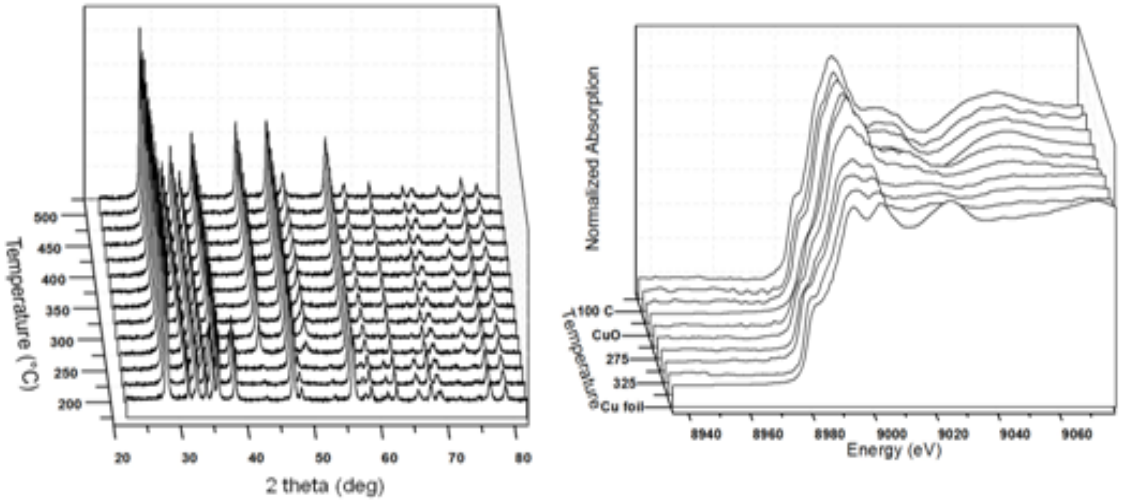


Figure 9: Left: In-situ XRD diffractograms and Right: normalized *in-situ* XANES transmission spectra at the Cu K-edge as a function of temperature for CZLL pyrochlores during $H_2$-TPR.

The CO adsorption properties of Mn and Co promoted Cu-ZnO-$La_2Zr_2O_7$-$Li_2O$ pyrochlore catalysts were investigated using DRIFTS coupled with a mass spectrometer at 1 bar. Mn promoter significantly influenced the CO adsorption on Cu-ZnO-$La_2Zr_2O_7$-$Li_2O$ pyrochlore, whereas the Co promoter affected only the product distribution. On the Mn-promoted catalyst (CMnZLL), $Cu^+$-carbonyl species were detected, whereas the partially stable linear carbonyl species on the unpromoted (CZLL) and Co-promoted (CCoZLL) catalysts indicated the presence

of both $Cu^+$ and $Cu^0$ sites. Carbonate/formate species were formed during CO adsorption due to the interaction of CO with either surface hydroxyl groups or with the residual hydrogen present after the reduction step. These species were reduced to formate/methoxy species upon hydrogenation at high temperatures, which are considered to be the intermediates for alcohol/oxygenate synthesis.

Mass spectrometer results indicated that the $C_{2+}$ alcohol/oxygenate formation on the Cu-ZnO-$La_2Zr_2O_7$-$Li_2O$ catalysts decreases in the following order under the tested reaction conditions: CMnZLL > CZLL > CCoZLL. Mass 15 (methane) was identified to be the major product on the Co-promoted catalyst and was present in the reaction product stream at concentrations around 100 times greater than that on the other two catalysts, whereas the Mn-promoted catalyst showed negligible methanation under the same conditions, consistent with the CO adsorption properties.

**(4) Co/CuZnO catalysts**

Based on BET analysis, XRD and TPR for Co/$Al_2O_3$, CuZnO, CoCu, CoZnO and Co/CuZnO, it was found that the different combinations of Cu, Zn and/or Co resulted in significant differences in surface area, structure, crystallite size, and reducibility for the catalysts. These catalysts also exhibited significantly different catalytic activities and selectivities for CO hydrogenation under FTS conditions. ZnO improved the dispersion of Co to some extent and might also enhance hydrogenation. Cu greatly enhanced reducibility of Co. Only the combination of all these three metal components, however, led to the formation of higher oxygenates with substantially higher selectivity. There appears to be no correlation of surface area, particle size and reducibility with activity and selectivity of the catalysts.

The relationships between the hydrocarbon and oxygenate products during CO hydrogenation on CoCuZnO-based catalysts were investigated for the first time at a site level using multiproduct SSITKA. By comparing the SSITKA results for the various catalysts, several conclusions can be made about the combination of Co with Cu and/or ZnO:

i. Cu alone acts to decrease activity of Co for all products, probably by blockage of the Co surface. Cu does not affect the intrinsic activities for either hydrocarbon or oxygenate formation based on the $TOF^0_{ITK}$'s.
ii. ZnO alone acts as a support (dispersion agent), keeping Co highly dispersed and very active for hydrocarbon synthesis. It appears to also possibly increase the site activities for $C_{2+}$ oxygenates.
iii. The combination of Cu and ZnO with Co appears to be able to maintain the oxygenate synthesis ability of highly dispersed Co (such as for Co/$Al_2O_3$) while simultaneously decreasing its ability to make hydrocarbons by loss of hydrocarbon synthesis sites.

Previous studies proposed that the combination of Co with CuZnO could effectively increase the selectivities for higher oxygenates due to the $C_1$-oxygenate sites (-$CH_xO$) contributed by CuZnO.

Higher alcohols were hypothesized to be formed through the reaction of a hydrocarbon species and a $C_1$-oxygente entity. The results from this study, however, indicate that Co (in the form of $Co/Al_2O_3$) already makes oxygenates including higher oxygenates. This fact tends to be overlooked due to the high hydrocarbon activity of $Co/Al_2O_3$.

It was found from SSITKA under methanation conditions that compared to Cu, the addition of ZnO to Co boosted the site activity to some extent while Cu seemed to have little effect on the activity of Co. The most pronounced differences for these catalysts were observed for the amounts of the reaction intermediates on the surface. The combination of Co with ZnO and/or Cu led to much decreased surface concentrations of reaction intermediates for $CH_4$. The results for ethane hydrogenolysis indicated that the different components for these multi-component catalysts were in close contact and few or no relatively large ensembles ($n \geq 12$) of Co atoms existed on the surface in these catalysts. Thus, it can be suggested that Co/CuZnO achieves its high selectivity for oxygenates by blockage of a significant portion of the hydrocarbon synthesis sites while retaining oxygenate synthesis sites, but at the cost of the high activity normally expected for Co catalysts.

**(5) CuZnO and $CuZnO/Al_2O_3$ on Methanol Synthesis: Analysis at the Site Level by SSITKA**

Two main issues were addressed using SSITKA: (1) the synergy between Cu and ZnO for MeOH synthesis on CuZnO or $CuZnO/Al_2O_3$; and (2) the change in the surface parameters for MeOH synthesis for CuZnO catalysts upon using an $Al_2O_3$ support. Even though the effects of different supports and components on CuZnO-based catalysts for MeOH synthesis have received a great deal of attention in the past, this study has explored for the first time at the reaction site level using SSITKA the impact of the components and a $Al_2O_3$-support on CuZnO-based catalysts.

CO hydrogenation results indicated that the overall reaction activity of CuZnO-based catalysts were higher than catalysts with only Cu or ZnO components but not orders of magnitude higher, indicating some synergy between Cu and ZnO species. DME is a secondary reaction product from the dehydration of MeOH and was produced only on the acidic sites of $Al_2O_3$ when it was present as a support.

The original SSITKA surface reaction parameters, $\tau_i$ and $N_i$, obtained from SSITKA were corrected for readsorption effects to $\tau^0_i$ and $N^0_i$. $\tau^0_{MeOH}$ (corrected average surface reaction residence time for MeOH formation) was essentially the same for both CuZnO and $CuZnO/Al_2O_3$, indicating that the $Al_2O_3$ support does not change the nature of active sites for the production of MeOH on CuZnO.

i. The reaction rates for MeOH formation on CuZnO and CuZnO/$Al_2O_3$ were nearly identical on a per g catalyst basis; however, on a per g CuZnO basis, CuZnO/$Al_2O_3$ had a much higher rate. This difference was due to the higher concentration of active surface intermediates/sites, almost certainly reflecting an increased dispersion of the supported CuZnO. The identical "site" activities seen for these 2 catalysts suggest that the sites, however, were identical for making MeOH. Thus, the only roles that the $Al_2O_3$ appeared to play was in increasing CuZnO dispersion and providing acid sites for the conversion of MeOH to DME.
ii. Using a support, higher dispersions of Cu and ZnO were possible (for Cu/$Al_2O_3$ and ZnO/$Al_2O_3$ catalysts) resulting in better comparisons to the CuZnO catalysts. Cu/$Al_2O_3$ and ZnO/$Al_2O_3$ exhibited lower MeOH formation rates compared to CuZnO/$Al_2O_3$ because of their lower intrinsic activities and lower surface concentrations of intermediates. It appear while there is some synergy between Cu and ZnO in producing MeOH on CuZnO catalysts, this synergy does not result in an order-of-magnitude increase in the site activity or active site concentration.
iii. Cu/$Al_2O_3$ was capable of producing significant hydrocarbon selectivity, but CuZnO/$Al_2O_3$ and ZnO/$Al_2O_3$ were not. This seems to imply that the presence of ZnO inhibits the hydrocarbon formation ability of Cu.

## Results and Discussion: Computational studies

### Adsorption of $H_2$ on small rhodium clusters

DFT calculations indicate that the initial adsorbate position parallel to one of the cluster three-fold faces is highly favorable for $H_2$ chemisorption consistent with previous calculations on metallic periodic surfaces. Terminal Rh-H bonds are only formed on $Rh_2$ and $Rh_3$ and the general rule for the rest of the clusters is the formation of bridge bonds. Adsorption on the four-fold sites of rhombic $Rh_4$ and square-based pyramidal $Rh_5$ only produced physisorbed structures, suggesting the activated nature of H-H breaking on these sites. For the rhombic $Rh_4$, the energy liberated in the interaction with H2 is -85.4 kJ/mol (which is comparable to the measured chemisorption energy for $H_2$ on polycrystalline rhodium) came from heavy relaxation of the surface into a tetrahedral structure. Apparently, our results on adsorption on four-fold sites apparently diverge from previous theoretical results that indicate the high adsorption energy of atomic H on rhodium surfaces and clusters. Chemisorption energies of $H_2$ on this cluster series are in the range from -20 to -124 kJ/mol and may come with significant changes in the structure of the host cluster as in the case of $Rh_9$.

Table 6: Calculated adsorption energies for $H_2$ on $Rh_5$, $Rh_7$, $Rh_8$, $Rh_9$, and characterization of the resulting adsorbate-metal complexes

| Rhodium cluster | Octahedral $Rh_6$ | Capped octahedron $Rh_7$ | | Pentagonal bipyramid $Rh_7$ | More stable $Rh_8$ | More stable $Rh_9$ |
|---|---|---|---|---|---|---|
| Initial $H_2$ position | Three-fold | Four-fold | Three-fold | Three-fold | Three-fold | Three-fold |
| Adsorption Energy, kJ/mol | -23.8 | -19.4 | -9.2 | -55.4 | -115.7 | -32.5 |
| Complex formula | $Rh_6(H)_2$ | $Rh_7(H)_2$ | $Rh_7(H)_2$ | $Rh_7(H)_2$ (B) | $Rh_8(H)_2$ | $Rh_9(H)_2$ |
| Spin multiplicity | 9 | 12 | 10 | 12 | 11 | 14 |
| S(S+1) | 20 | 35.75 | 24.75 | 35.75 | 30 | 48.75 |
| $S^2$ | 20.154 | 35.894 | 24.985 | 35.902 | 30.215 | 48.938 |
| Complex symmetry | | | | | | |
| initial | $C_1$ | $C_1$ | $C_1$ | $C_1$ | $C_1$ | $C_1$ |
| final | $C_1$ | $C_1$ (off) | $C_1$ (off) | $C_1$ | $C_1$ | $C_1$ |
| Orbital energy, Hartree | | | | | | |
| HOMO | -0.172 | -0.167 | -0.171 | -0.177 | -0.162 | -0.180 |
| LUMO | -0.119 | -0.116 | -0.124 | -0.124 | -0.125 | -0.119 |
| Average bond length, Å | | | | | | |
| Rh-Rh | 2.67 | 2.64 | 2.64 | 2.67 | 2.67 | 2.67 |
| Rh-H | 1.71 | 1.82 | 1.78 | 1.74 | 1.69 | 1.73 |
| H-H | 2.34 | 0.81 | 0.84 | 2.67 | 2.30 | 2.17 |

### Adsorption of CO on small rhodium clusters

DFT studies were carried out to study the relative selectivity of CO for adsorption on terminal, bridge and three-fold sites of small $Rh_n$ clusters ($2 \leq n \leq 10$). The metal clusters and the $Rh_nCO$ complexes were fully optimized at the B3LYP/LACVP Density Functional Theory level. The results show that the energy of CO adsorption on the three-fold sites decreases with the number of metal atoms in the cluster and adsorption on the terminal and bridge sites becomes dominant.

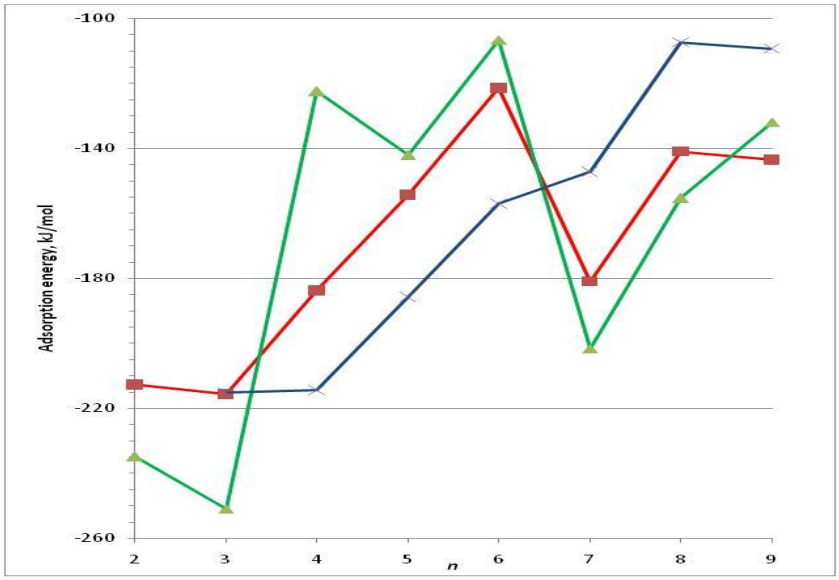

Figure 10: Maximum calculated adsorption energies of CO on $Rh_n$ clusters. The red, green, and blue lines indicate CO bound to terminal, bridge, and three-fold sites.

**Adsorption of CO on $Rh_7$ pre-adsorbed with $(H)_2$**

When CO is adsorbed on rhodium cluster ($Rh_7$) pre-adsorbed with $(H)_2$, an increase in the average H-Rh bond length ensues suggesting that H atoms become more available for further reaction. The effect of La model species on the adsorption of CO and H on $Rh_7$ was also determined. LaO(OH) was found to induce the reorientation of CO and the distortion of cluster geometry. It was found that CO adsorbs molecularly and $H_2$ dissociates on both the $Rh_7$ cluster and the $Rh_7$/LaO(OH) complex. The presence of LaO(OH) near the adsorption sites of H atoms and CO affects the equilibrium positions of these adsorbates.

**Adsorption of CO and $H_2$ on Co-Pd metal clusters**

Binary Co-Pd metal clusters of the general form CoxPdy (x + y=13), which is a 13 atom icosahedral structure (one atom in center and twelve on surface), serve to model the active sites in the prepared bulk catalysts. DFT simulations of CO adsorption on the terminal, bridge and threefold sites of Co-Pd binary cluster with the formula CoxPdy (x+y=13, 0=x<=13) show the adsorption energies of CO varying in a saw-tooth pattern. Our calculations show that the CO chemisorptions are very stable in Pd rich region (x<=4). For adsorption position, CO prefers bridge adsorption sites in Pd rich region. However, as the ratio of Co atoms in the cluster increases (x>4), the bridge site and threefold site adsorptions become less relevant. It is believed that the hydrogenation reactions premises on the chemisorptions of both carbon monoxide and hydrogen. Too strong adsorptions of CO might prevent the adsorptions of $H_2$, thus hinder the

activation of hydrogenation reaction. So it is suggested here Co rich clusters could be the more active catalysts in the Co-Pd binary mixtures.

The hydrogen dissociative adsorption energy on selected $Co_xPd_y$ (x + y =13, x<=3) clusters was also examined. It was clear that the chemisorption of $H_2$ was more stable than physisorption because the process of breaking a chemical bond is exothermic. Also, from the results, the chemisorption of $H_2$ was very stable on Pd 13, Co1Pd12, Co2Pd11 and Co3Pd10 clusters and, thus, the chemisorption of $H_2$ was unlikely to be a rate limiting step on these four clusters.

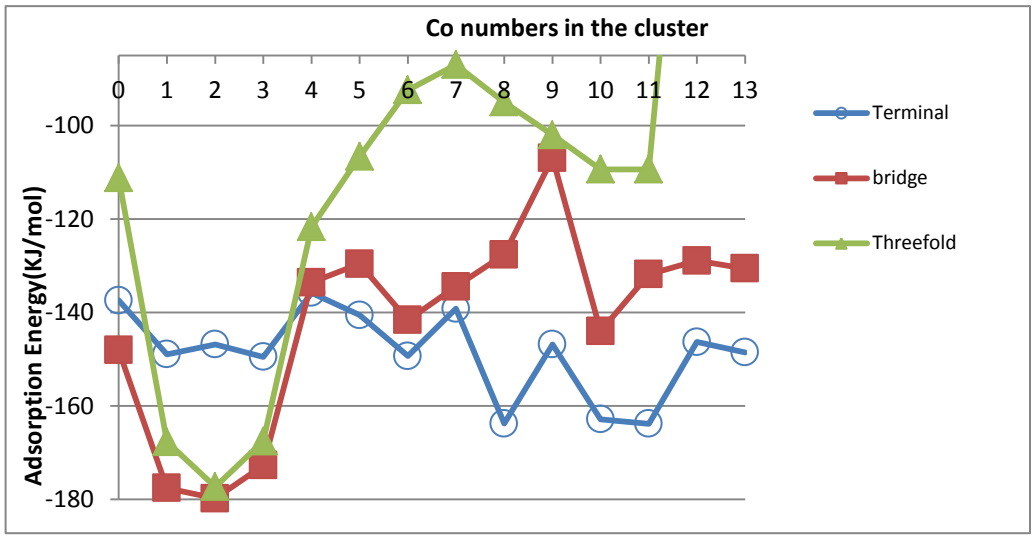


Figure 11: CO adsorption energies on the CoxPdy clusters

# Results and Discussion: Process economics study

## Summary

Hysys process simulation software was used to design a conceptual, 10,000 TPD Coal-to-Ethanol plant to evaluate the economic impact of varying the performance of several process variables associated with the ethanol reactor. The variables explored in these simulations were ethanol selectivity, quantity of hydrogen produced by water gas shift, CO conversion per pass, reactor pressure and selectivity toward alkane production. The coal of choice was Illinois #6 with (11.12% moisture content) which was assumed to be converted to syngas using the ConocoPhillips' E-Gas gasification process.

Experimental assumptions:

1. Power to be purchased, thus saving syngas for process use.
2. A pressure swing adsorption (PSA) unit has been added to extract hydrogen from the reactor recycle stream.
3. Steam is added to the syngas that feeds the reaction, even although the LSU experiment does not include such an addition. The change may lead to results not in accord with original experimental data. The economics and the supporting simulation assume that instead of carbon being deposited on the catalyst, both $CO_2$ and hydrogen are produced as products of the WGS reaction and that the yields of alcohols are unaffected.
4. Rectisol units for carbon dioxide removal from reactor recycle are retained in this process scheme, but the increased amount of carbon dioxide has been provided for with additional equipment and operating cost.
5. The cost of catalyst is based on refined lanthanum. It is likely that an oxide would be much less expensive. Cost of preparation of catalyst is not considered.

Catalysts used for economic study: 1.5% Rh-La/V/$SiO_2$ and Cu-Mn-ZnO-$La_2Zr_2O_7$-$Li_2O$.

**Rh-La-V-$SiO_2$ catalyst:**

For the Rh-based catalyst, the production cost of ethanol (without subsidy) ranged from $2.20 to $3.70/gal (depending on assumptions), which is competitive with current market costs and to costs estimated by DoE for thermochemical processes (Phillips et al., NREL/TP-510-41168, April 2007).

A reactor design that minimizes the required catalyst inventory is critical to the economic success of this project. This is especially true for the 2 wt% rhodium catalyst that was used in the Base Case experimental run. Rhodium is more costly than platinum or gold and has been running close to $1,100 per troy ounce. A reactor design that utilizes fluidized beds for both ethanol production and catalyst regeneration (which is assumed to involve burning off coke) is considered to be the only viable option because it can allow for much smaller catalyst inventory than could a fixed bed design. Because it is common for fluidized catalytic cracking (FCC) units, a gasoline-producing unit common in oil refineries, to have a cycle times as low as five minutes, that assumption is also applied to the ethanol reactor.

Cycle time is the time required for a catalyst particle to enter the reactor, pass through the reactor and regenerator and return to the inlet of the reactor. Assuming that 37% loss of activity is acceptable for the catalyst particle entering the regenerator then, for a five minute cycle time, the ratio of CO converted to product over weight of catalyst is 1/1. For the 2 wt% rhodium catalyst that is converting 420,000 lb/hr of CO, the catalyst inventory cost would be $144 million. Though this is a large expense, it is less than 5% of the total plant investment. Fixed bed reactors, that typically have cycle times measured in weeks or months, would be entirely impractical for this application.

Regeneration is assumed to be accomplished by the burning off of coke that has settled upon and deactivated the catalyst. It is also critical to the success of this project that the catalyst can be fully regenerated many, many times over. A five minute cycle time would result in 288 regenerations per day and 105,120 times per year. Fluidized beds do suffer catalyst loss due to attrition. Based on analogies with FCC units, the attrition losses for the rhodium based catalyst is estimated to be $18 million per year, which is about 5% of total plant operating costs. See 4Q2008 quarterly report for complete details.

**Cu-Mn-ZnO-$La_2Zr_2O_7$-$Li_2O$ catalyst:**

Lanthanum makes up 89% of the catalyst cost. Due to the high cost of lanthanum, estimated to be $210/kg, coupled with methanol, as opposed to more valuable $C_{2+}$ alcohols, comprising 80 liquid volume % of all alcohols produced, a plant build upon this technology would fall well short of economic viability. For a conceptual plant that feeds syngas produced by the gasification

of 10,000 TPD of Illinois #6 coal to achieve breakeven economics, the ethanol, which makes up only 17 LV% of the alcohols produced, would have to sell for $11.13/gallon. This compares to ethanol's current market price of ~$2.50/gallon.

Further challenges to the economics are the high amount of $CO_2$ the catalyst produces and the related oxygen-to-carbon ratio in the products, which suggests that a significant amount of carbon may be coking out on the catalyst. Of the carbon, which originates with the CO component of the syngas, 43% is lost to $CO_2$, which steals away carbon that would have had value if converted into alcohols.

Because methanol is the primary product of this catalyst, the economics of the plant modeled in this study were compared with those of a methanol plant based on technology commercialized by Haldor Topsoe as reported by SRI. Given an identical syngas stream, the Haldor Topsoe technology, which produces only methanol, would generate 91% of the revenue of the LSU-catalyst-based plant with only 20% of the capital investment and 25% of the operating cost. See 2Q2011 quarterly report for complete details.

**Comparison between Rh and Cu based catalysts on the cost of ethanol production:**

The $11.13 per gallon cost for the copper catalyst is 3–4 times higher than the costs for the Rh-based catalyst. Reasons for this apparent increase are as follows:

1. The very large fixed-bed reactors are costly, primarily due to the cost of lanthanum.

2. A five-fold increase in $CO_2$ production (up to 54.5% from 10.6%) not only steals carbon away from alcohol synthesis but also is costly to remove. The power needed for refrigeration in the Rectisol unit is 97 MW, which is nearly half of the plant's total power requirement.

3. The methanol/ethanol molar ratio increased from 1.44 to 2.68. This lower ethanol yield (relative to methanol), together with the ASTM D-5501 specification for fuel grade ethanol that limits methanol to not more than 0.5%, resulted in increased fractionation costs. Fractionating these products, even when 5.0 LV % ethanol is allowed to slip into the methanol product, required a boiler duty at the methanol separation tower that was comparable to the heating value of the final ethanol product.

4. Also related to the lower yield of ethanol is the fact that the model is less sensitive to its price variations. To achieve break-even economics while holding all other product prices constant at their 2011 values, the price of ethanol had be adjusted upward significantly.

5. The contingencies applied to the cost in the earlier study were unrealistically low, especially when considering the unproven nature of the fluidized bed system with rapid

regeneration that was proposed in the study. New protocols for determining contingencies for non-commercialized processes would have increased that earlier estimate by at least 50%.

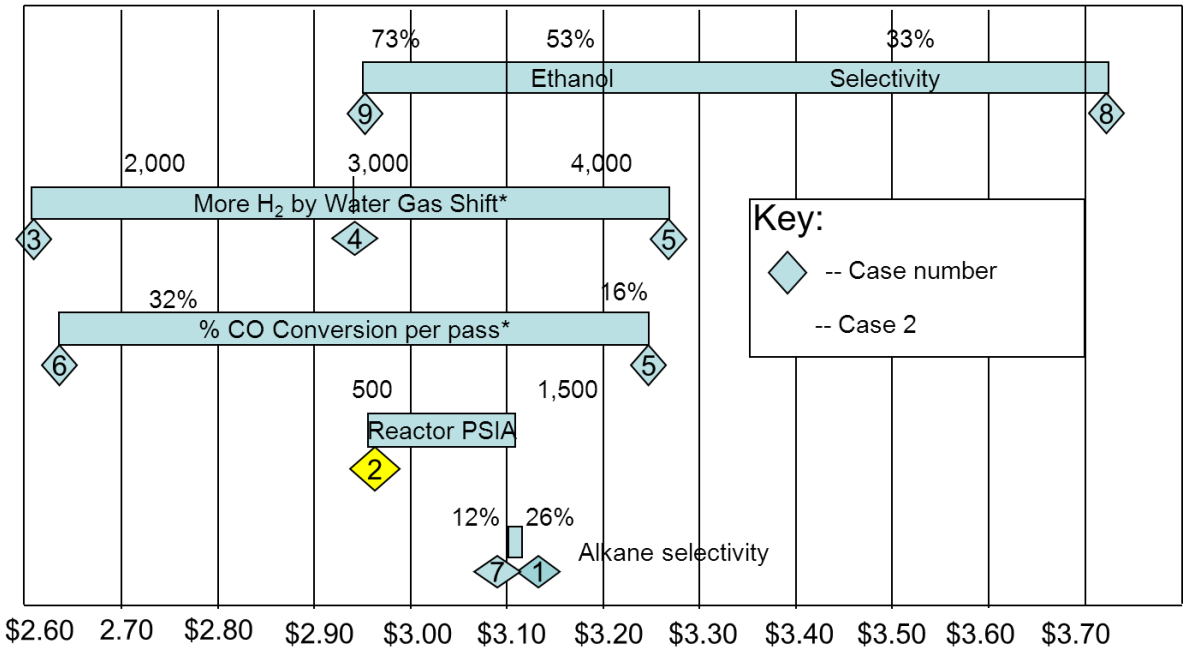


Figure 12: Sensitivities of costs to process variables – Rh-La/V/$SiO_2$ catalyst

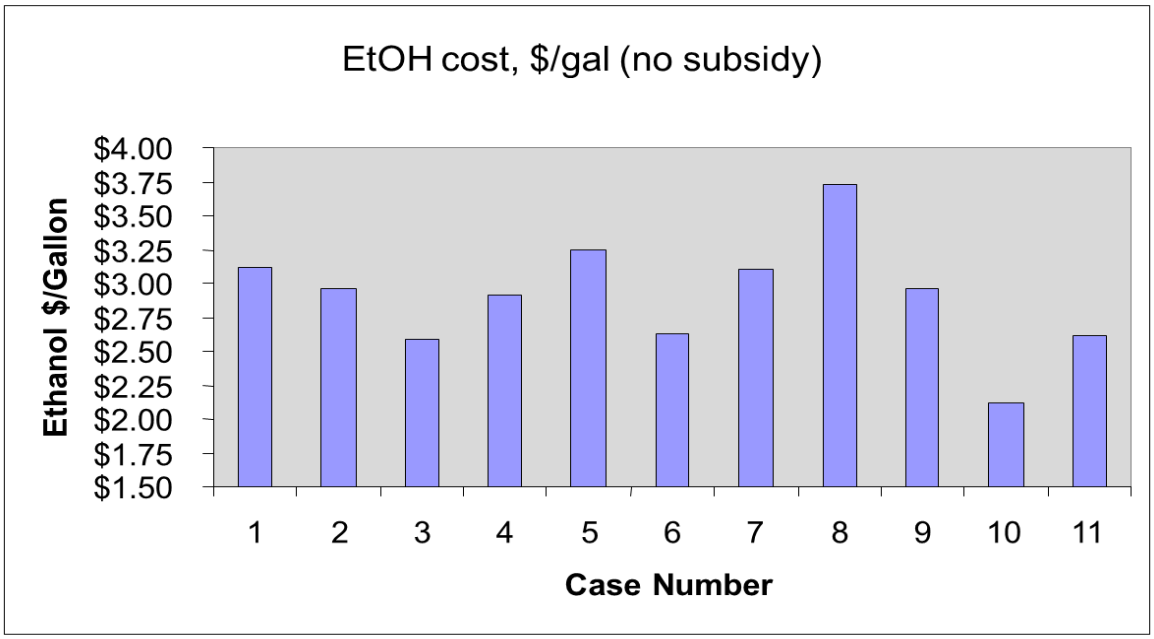


Figure 13: Ethanol cost per gallon, without subsidy – Rh-La/V/$SiO_2$ catalyst

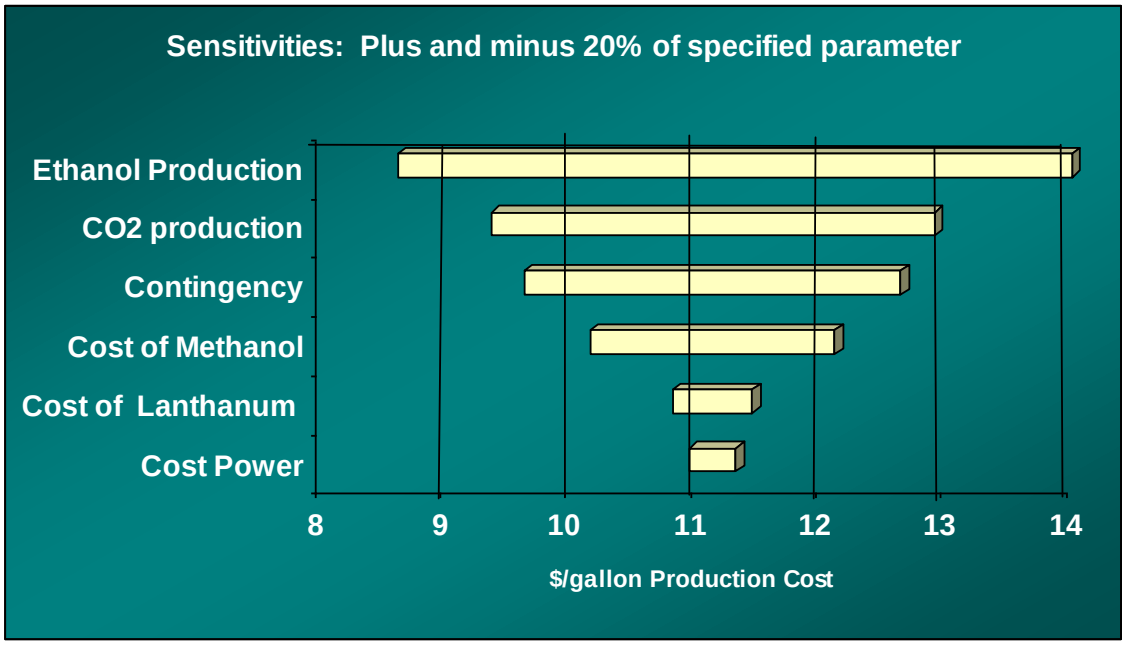


Figure 14: Sensitivities of costs to process variables – Cu-Mn-ZnO-$La_2Zr_2O_7$-$Li_2O$ catalyst

# Appendix-I: Cost report

U. S. Department of Energy
Award # DE-FC26-06NT43024
LSU account # 127-10-5161
As of 6/30/11

**COST PLAN/STATUS**

| | Year 1 Start: 10/01/06 End: 09/30/07 | | | | Year 2 Start: 10/01/07 End: 09/30/08 | | | | Year 3 Start: 10/01/08 End: 09/30/09 | | | | Year 4 Start: 10/1/09 End: 09/30/2010 | | | | Year 5 Start: 10/1/2010 End: 07/29/2( | | |
|---|---|---|---|---|---|---|---|---|---|---|---|---|---|---|---|---|---|---|---|
| **Baseline Reporting Quarter** | Q1 | Q2 | Q3 | Q4 | Q5 | Q6 | Q7 | Q8 | Q9 | Q10 | Q11 | Q12 | Q13 | Q14 | Q15 | Q16 | Q17 | Q18 | Q19 |
| **Baseline Cost Plan (from SF-424A)** | | | | | | | | | | | | | | | | | | | |
| Federal Share | 206,000.00 | 116,000.00 | 153,538.00 | 153,538.00 | 137,800.00 | 137,800.00 | 137,800.00 | 137,800.00 | 149,905.75 | 149,905.75 | 149,905.75 | 149,905.75 | - | - | - | - | - | - | - |
| Non-Federal Share | 77,515.50 | 77,515.50 | 77,515.50 | 77,515.50 | 74,822.50 | 74,822.50 | 74,822.50 | 74,822.50 | 73,806.75 | 73,806.75 | 73,806.75 | 73,806.75 | - | - | - | - | - | - | - |
| Total Planned (Federal and Non-Federal) | 283,515.50 | 193,515.50 | 231,053.50 | 231,053.50 | 212,622.50 | 212,622.50 | 212,622.50 | 212,622.50 | 223,712.50 | 223,712.50 | 223,712.50 | 223,712.50 | - | - | - | - | - | - | - |
| Cumulative Baseline Cost | 283,515.50 | 477,031.00 | 708,084.50 | 939,138.00 | 1,151,760.50 | 1,364,383.00 | 1,577,005.50 | 1,789,628.00 | 2,013,340.50 | 2,237,053.00 | 2,460,765.50 | 2,684,478.00 | 2,684,478.00 | 2,684,478.00 | 2,684,478.00 | 2,684,478.00 | 2,684,478.00 | 2,684,478.00 | 2,684,478.00 |
| **Actual Incurred Costs** | | | | | | | | | | | | | | | | | | | |
| Federal Share | 4,584.11 | 28,709.22 | 78,444.79 | 198,163.22 | 16,736.93 | 128,971.14 | 136,328.04 | 193,248.10 | 71,415.03 | 130,307.16 | 97,101.85 | 154,880.41 | 139,681.58 | 89,451.50 | 19,516.81 | 131,606.95 | 91,442.38 | 60,404.26 | 8,905.52 |
| Non-Federal Share | - | 21,589.75 | - | 21,589.75 | - | 82,100.99 | - | 274,738.32 | 3,521.30 | 61,108.33 | - | - | - | - | 654.78 | - | - | - | 558,217.00 |
| otal Incurred Costs-Quarterly (Federal and Non-Federal) | 4,584.11 | 50,298.97 | 78,444.79 | 219,752.97 | 16,736.93 | 211,072.13 | 136,328.04 | 467,986.42 | 74,936.33 | 191,415.49 | 97,101.85 | 154,880.41 | 139,681.58 | 89,451.50 | 20,171.59 | 131,606.95 | 91,442.38 | 60,404.26 | 567,122.52 |
| Cumulative Incurred Costs | 4,584.11 | 54,883.08 | 133,327.87 | 353,080.84 | 369,817.77 | 580,889.90 | 717,217.94 | 1,185,204.36 | 1,260,140.69 | 1,451,556.18 | 1,548,658.03 | 1,703,538.44 | 1,843,220.02 | 1,932,671.52 | 1,952,843.11 | 2,084,450.06 | 2,175,892.44 | 2,236,296.70 | 2,803,419.22 |
| **Variance** | | | | | | | | | | | | | | | | | | | |
| Federal Share | 201,415.89 | 87,290.78 | 75,093.21 | (44,625.22) | 121,063.07 | 8,828.86 | 1,471.96 | (55,448.10) | 78,490.72 | 19,598.59 | 52,803.90 | (4,974.66) | (139,681.58) | (89,451.50) | (19,516.81) | (131,606.95) | (91,442.38) | (60,404.26) | (8,905.52) |
| Non-Federal Share | 77,515.50 | 55,925.75 | 77,515.50 | 55,925.75 | 74,822.50 | (7,278.49) | 74,822.50 | (199,915.82) | 70,285.45 | 12,698.42 | 73,806.75 | 73,806.75 | - | - | (654.78) | - | - | - | (558,217.00) |
| Total Variance-Quarterly (Federal and Non-Federal) | 278,931.39 | 143,216.53 | 152,608.71 | 11,300.53 | 195,885.57 | 1,550.37 | 76,294.46 | (255,363.92) | 148,776.17 | 32,297.01 | 126,610.65 | 68,832.09 | (139,681.58) | (89,451.50) | (20,171.59) | (131,606.95) | (91,442.38) | (60,404.26) | (567,122.52) |
| Cumulative Variance | 278,931.39 | 422,147.92 | 574,756.63 | 586,057.16 | 781,942.73 | 783,493.10 | 859,787.56 | 604,423.64 | 753,199.81 | 785,496.82 | 912,107.47 | 980,939.56 | 841,257.98 | 751,806.48 | 731,634.89 | 600,027.94 | 508,585.56 | 448,181.30 | (118,941.22) |